IEEE Photonics Journal
An IEEE Photonics Society Publication

Open Access

Surface Brillouin Scattering in Disordered Optical Fibers With Transverse Anderson Localization Guiding Mechanism for Evaluation of Longitudinal Structural Fluctuations

Volume 10, Number 1, February 2018

Sheng Liang
Yongxin Zhang
Xin Wang
Xinzhi Sheng
Shuqin Lou
Bo Lin
Mingli Dong
Lianqing Zhu

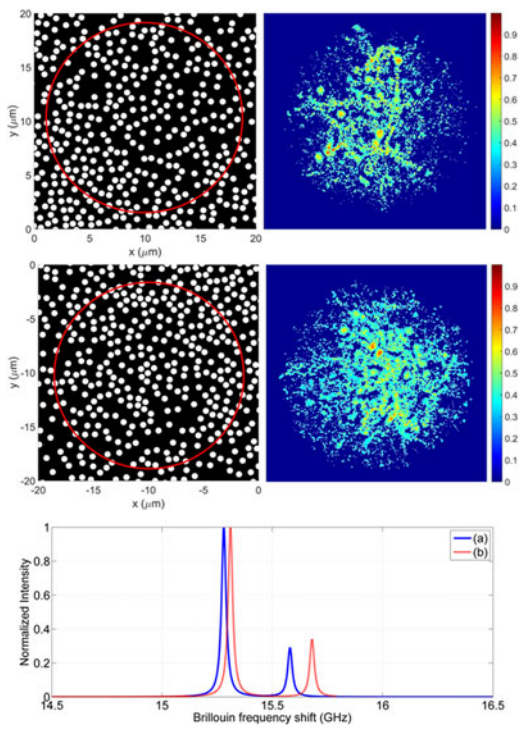

DOI: 10.1109/JPHOT.2018.2793868
1943-0655 © 2018 IEEE

Surface Brillouin Scattering in Disordered Optical Fibers With Transverse Anderson Localization Guiding Mechanism for Evaluation of Longitudinal Structural Fluctuations

Sheng Liang,[1] Yongxin Zhang,[1] Xin Wang,[2] Xinzhi Sheng,[1] Shuqin Lou,[2] Bo Lin,[3] Mingli Dong,[4] and Lianqing Zhu[4]

[1]Key Laboratory of Education Ministry on Luminescence and Optical Information Technology, National Physical Experiment Teaching Demonstration Center, Department of Physics, School of Science, Beijing Jiaotong University, Beijing 100044, China
[2]School of Electronic and Information Engineering, Beijing Jiaotong University, Beijing 100044, China
[3]China Academy of Electronics and Information Technology, Beijing 100041, China
[4]Beijing Key Laboratory for Optoelectronics Measurement Technology, Beijing Engineering Research Center of Optoelectronic Information and Instruments, Beijing Information Science and Technology University, Beijing 100016, China

DOI:10.1109/JPHOT.2018.2793868

Manuscript received November 20, 2017; revised December 29, 2017; accepted January 11, 2018. Date of publication January 15, 2018; date of current version January 25, 2018. This work was supported in part by the National Natural Science Foundation of China (no. 61675019), in part by the Program for Changjiang Scholars and Innovative Research Team in University under Grant no. IRT_16R07, and in part by the National Key R&D Program of China (2016YFC0800500). (Sheng Liang and Yongxin Zhang contributed equally to this work.) Corresponding author: Xinzhi Sheng (e-mail: xzhsheng@bjtu.edu.cn).

Abstract: We numerically investigate the surface Brillouin scattering (surface-BS) in a transverse Anderson localization (TAL) guiding silica glass-air disordered optical fiber (DOF) with random air-holes. The normalized light intensity profiles of light beams propagating along DOF at different launch positions are obtained, which confirms the TAL mechanism. Then, the surface-BS in DOF is numerically investigated by the equation of elastodynamics with the electrostriction. It is found that there are two main peaks in the surface-BS spectrum and the Brillouin frequency shift (BFS) is sensitive to the air-fill fraction of DOF. Furthermore, the feasibility of longitudinal structural fluctuations evaluating of DOF by the Brillouin optical time-domain analysis technique is analyzed and discussed. The average sensitivity of BFS to the air-fill fraction is simulated to obtain an optimal performance in practical application. This paper is an interesting theoretical enlightenment for combining the novel concepts of surface-BS and DOF, also a useful exploration of longitudinal structural evaluating method for special optical fibers with microstructures.

Index Terms: Disordered optical fiber (DOF), transverse Anderson localization (TAL), surface Brillouin scattering (surface-BS), longitudinal structural fluctuations evaluation.

1. Introduction

As a novel optical fiber, the disordered optical fiber (DOF) has attracted significant research interests [1]–[3] due to the peculiar wave-guiding mechanism, i.e., transverse Anderson localization (TAL)

[4]–[10]. The conventional optical fibers are based on the index-guiding mechanism, however, DOF are based on the strong multiple scattering across due to the TAL, which can guide a light beam launched at any positions across the transverse profile of a DOF. This interesting property can be used for potential applications in multiple-beam propagation for spatially multiplexed fiber-optic communications, and imaging transmission with improved resolution [4]–[10].

Two important parameters for DOF are the localization beam radius (also called localization length, or effective beam radius) and its sample-to-sample variation. A polymer DOF is proposed and fabricated by polystyrene (PS) with refractive index $n = 1.59$ and poly (methyl methacrylate) (PMMA) with $n = 1.49$ [4]. The average localization beam radius $\xi_{ave} = 31\,\mu$m, with a standard deviation $\sigma_\xi = 14\,\mu$m are observed. However, this variation of localization beam radius can be reduced by increasing the index difference between the random sites of the DOF or operating at a shorter incident wavelength [5]. Compared with the polymer DOF, the silica glass-air DOF can bring in smaller localization beam radius, and the lower sample-to-sample variation, due to the increased refractive index contrast in fused silica to air structure. Therefore, more research work will be focused in silica glass-air DOFs in future.

Currently, the transverse localization of light beam in DOF is observed experimentally to be less than 100 cm, i.e., $\approx$60 cm for polymer DOF [4], [5] and $<$10 cm for glass DOF [6], and the longer propagation is affected by large longitudinal variations of the DOF structure during the draw process [4]–[6]. This short propagation limits the potential applications. Therefore, it is necessary to monitor the longitudinal structural fluctuations of DOF during the draw process.

To date, the structural properties of micro-structured optical fibers have typically been evaluated by high resolution microscopy, such as SEM. However, these destructive measurements cannot provide any information about the structural fluctuations along the fiber length. The Brillouin scattering characteristics of fibers are sensitive functions of the structural and optical parameters. A photonic crystal fiber (PCF) mapping method using backward Brillouin scattering was proposed [11]. It is found that the Brillouin frequency shift (BFS) is sensitive to the PCF microstructure. By Brillouin echoes distributed sensing with a high spatial resolution of 30 cm, the BFS along the fiber can be mapped to evaluate the longitudinal fluctuations of PCF [11].

For some optical fibers with sub-wavelength micro-structures, a novel Brillouin scattering, namely surface Brillouin scattering (surface-BS) is generated by the coupling between light wave and surface acoustic-wave (SAW) [12]–[14], and it seems to be a possible method to quantitatively estimate the longitudinal structural fluctuations of DOFs during the draw process.

The intention of this paper is to illuminate surface-BS in silica glass-air DOF with random air-holes and sub-wavelength scale structures. The relationships between surface-BS and structure parameters of DOF are numerically obtained. Then, the feasibility of longitudinal structural fluctuations evaluating by surface-BS based Brillouin optical time-domain analysis (BOTDA) technique are analyzed and discussed.

2. The Silica Glass-Air DOF

The structure of the silica glass-air DOF investigated in this paper is shown in Fig. 1, where there are a certain number of air-holes in the across of a fused silica host, randomly. This DOF can be fabricated by drawing a preform obtained by stretching the glass rod with random bubbles. Furthermore, the preform can be fabricated by mechanical drilling [15], stacking-fusing-etching [16], and die-cast process [17]. Interestingly, the preform by soft glasses, silica, and other materials can be fabricated more conveniently by the 3D printing technology, in the not-so-distant future [18]. The diameters of DOF and hole are $d_{DOF} = 125\,\mu$m, and $d_{hole} = 0.6\,\mu$m, respectively. The minimum air-hole pitch $\Lambda = 1.23\,\mu$m. Then, the minimum thickness of fused silica is $\Lambda - 2d_{hole} = 0.03\,\mu$m, and the minimum distance from air-hole center to the edge of DOF is $d_{hole}/2 = 0.3\,\mu$m. The geometry size of DOF is a probable scale for surface-BS [12], [13]. The index contrast is the fused silica ($n_1 \approx 1.5$) to air ($n_2 = 1.0$). The equivalent air-fill fraction p is the area ratio of the total air-holes to the whole DOF, and can be defined as:

$$p = S_{holes}/S_{DOF} \tag{1}$$

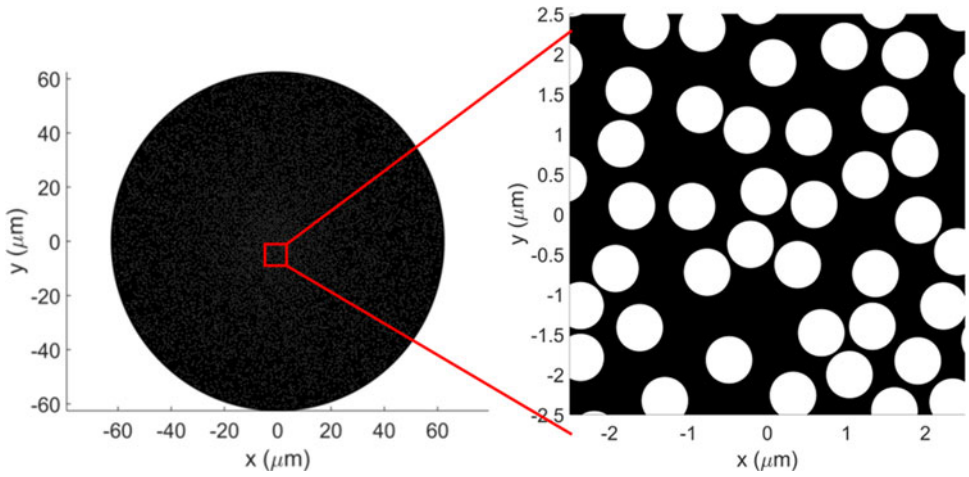

Fig. 1. The across structure of the silica glass-air DOF with random air-holes. The black background is fused silica host, and the white dots are the random air-holes.

where S_{holes}, and S_{DOF} are the total across area of air-holes and the whole DOF, respectively. For DOF shown in Fig. 1, $p = 18\%$, and the number of air-holes is 7812.

The propagation of light beams in DOF can be numerically simulated by the finite difference beam propagation method (FD-BPM) [5], [19]. The paraxial approximation to the *Helmholtz* equation is given by:

$$i\frac{\partial A}{\partial z} + \frac{1}{2n_0k_0}\left[\nabla_T^2 A + k_0^2\left(n^2 - n_0^2\right)A\right] = 0 \tag{2}$$

where $A(r)$ is the slowly varying envelope of the primarily transverse electric field:

$$E(r, t) = Re[A(r)\exp(in_0k_0z - i\omega t)] \tag{3}$$

which is centered around frequency ω, and $k_0 = 2\pi/\lambda$. $n(x, y)$ is the refractive index, as a function of the x–y coordinates. n_0 is the average refractive index of DOF. In the simulation, a monochromatic *Gaussian* beam with radius w is launched into a position of DOF at $z = 0$. The forward propagation can be implemented by the 4th-order *Runge–Kutta* method [20]. The localization beam radius can be calculated by the variance method [21], [22]:

$$\xi(z) = \sqrt{\left\langle A(r)\left|\left(R - \bar{R}\right)^2\right|A(r)\right\rangle} \tag{4}$$

where the angle brackets denote integration over x–y coordinates. $R = (x, y)$ is the transverse position vector, and $\bar{R}$ is the vector pointing to the center of the beam, defined as the mean intensity position. The optical field is assumed to be normalized, and the total power of Anderson localized beams remains unchanged during the propagation in the simulation.

Two incident 632.8 nm *Gaussian* beams with an initial full-width at half-maximum of 5 μm are launched into 2 positions across DOF. The normalized intensity profiles after 2 mm propagation are shown in Fig. 2. The strong transverse scattering results in transversely confined beams that can freely propagate in the longitudinal direction, with the advantage that any point in the cross section can be used for beam transport. In Fig. 2(a) and (b), $\xi_a = 8.80\,\mu$m, and $\xi_b = 8.62\,\mu$m, respectively. The TAL mechanism is a statistical phenomenon based on multiple random scattering, and the light propagation at different positions may be different. It is clearly that TAL is sensitive to the air-fill fraction p [4], [5], The localized beam radius in Fig. 2 are different, due to the different equivalent local air-fill fractions, which are $p_a = 25.7\%$, and $p_b = 28.2\%$, respectively. The higher equivalent local air-fill fraction 28.2%, results in a smaller localized beam radius 8.62 μm as shown in Fig. 2(b).

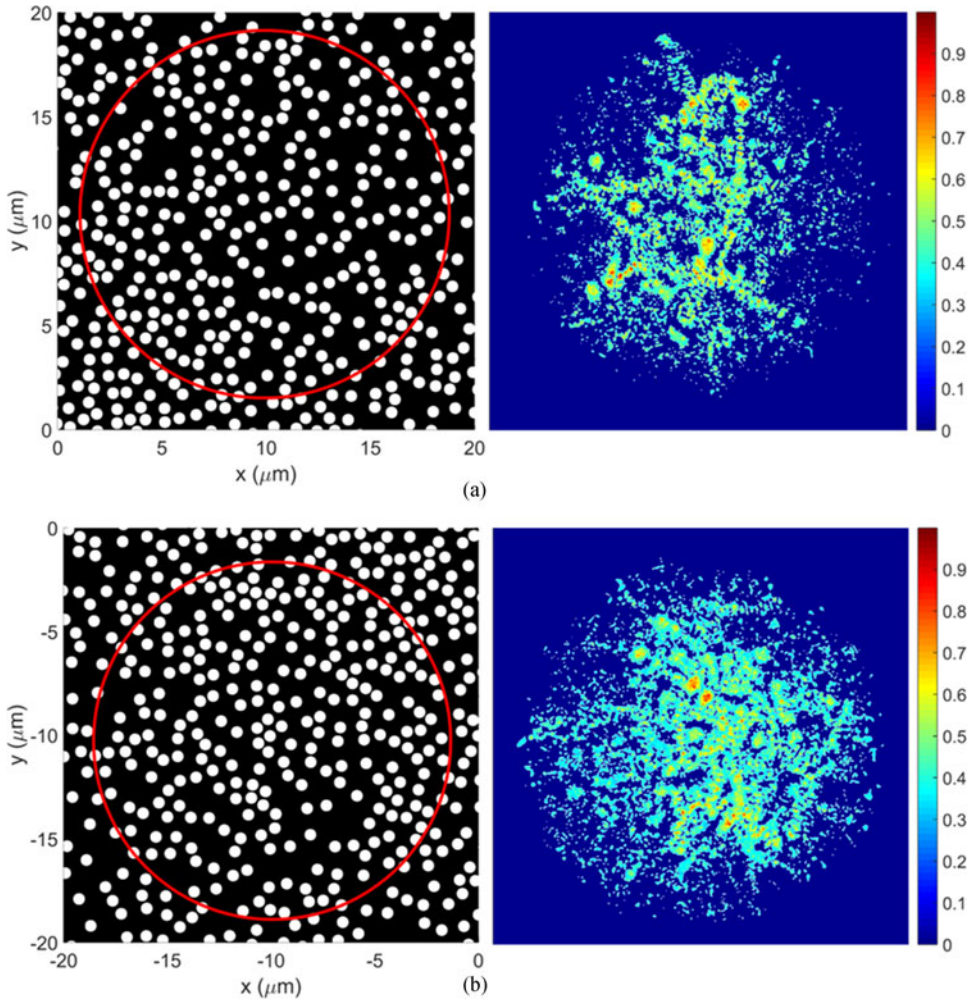

Fig. 2. The normalized intensity profiles after 2 mm of propagation along DOF at 2 different launch positions (a) and (b), $\xi_a = 8.80\,\mu$m, $\xi_b = 8.62\,\mu$m, $p_a = 25.7\%$, and $p_b = 28.2\%$.

3. Surface Brillouin Scattering in DOF

Unlike Brillouin scattering owing to the bulk acoustic waves, surface-BS is the scattering of light by SAWs [12]–[14]. Particularly in sub-wavelength scale structures, the phonons at the surface can bring in corrugation of the surface, which enables a strong opto-acoustic coupling between light and SAWs. The surface-BS in DOF can be described by the equation of elasto-dynamics with the electrostriction:

$$\rho \frac{\partial^2 u_i}{\partial t^2} - \frac{\partial}{\partial x_j}\left(c_{ijkl}\frac{\partial u_k}{\partial x_l}\right) = \frac{\partial}{\partial x_j}\varepsilon_0 \chi_{klij}\left[E_k E_l^*\right] \tag{5}$$

where u_i are the displacements, and C_{ijkl} is the rank-4 tensor of elastic constants. The right side of (5) is the electrostrictive stress, including the rank-4 susceptibility tensor $\chi_{klij} = \varepsilon_{km}\varepsilon_{ln}p_{mnij}$ with p_{mnij} the elasto-optic tensor, and ε_0 is the permittivity in vacuum. E_k and E_l are the pump and Brillouin Stokes fields with angular frequencies $\omega_{1,2}$ and axial wave vectors $k_{1,2}$. By solving (5) for the backward case numerically, the elastic energy density inside DOF can be obtained.

The distribution of electrostrictive stress follows the optical field distribution, without extending out of the silica. Then, as shown in Fig. 3, the elastic energy density is mainly localized in the thin solid silica, which can be considered as the surface of a solid silica cylinder. Thin solid silica and

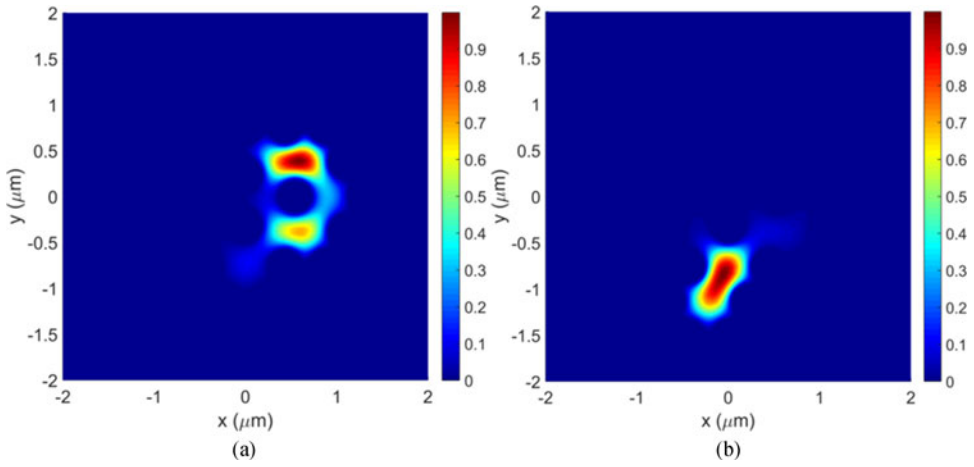

Fig. 3. The kinetic energy densities at 2 different launch positions in DOF.

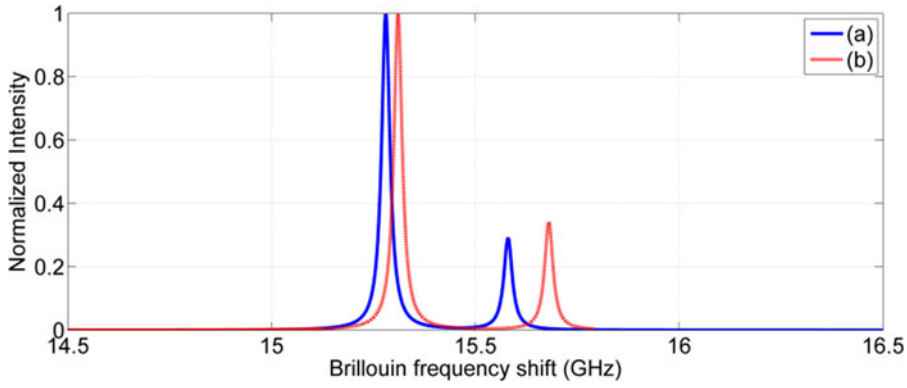

Fig. 4. Normalized surface-BS spectrums at 2 different launch positions in DOF. $\nu_{Ba1} = 15.28$ GHz, $\nu_{Ba2} = 15.58$ GHz, $p_a = 28.8\%$, $\nu_{Bb1} = 15.31$ GHz, $\nu_{Bb2} = 15.68$ GHz, and $p_b = 26.3\%$.

high air-fill fraction structure of DOF can realize a strong opto-acoustic coupling near the air-holes while mitigating the acoustic leakages.

By calculating the spatial overlap between the optical fundamental modes and the surface acoustic modes, we can obtain the normalized surface-BS spectrums at 2 different launch positions in DOF, as shown in Fig. 4. The interesting fact is that there is a dual-peak spectrum: the first peak, and a second peak on the high-frequency side, corresponding to the fundamental and the relevant higher-order surface acoustic modes. For simplicity, we ignore other high-order acoustic modes because only a small number of acoustic modes are responsible for the main peaks. The BFS for the first and second peaks at **(a)** and **(b)** launch positions are as follows: $\nu_{Ba1} = 15.28$ GHz, $\nu_{Ba2} = 15.58$ GHz, $\nu_{Bb1} = 15.31$ GHz, and $\nu_{Bb2} = 15.68$ GHz, respectively. The two peaks have both approximate *Lorentzian* shapes with the same bandwidth of ~23 MHz, in agreement with the phonon lifetime in fused silica ~10 ns, which is assumed to be equal for all the acoustic modes in simulation. Analytically, BFS is proportional to the effective refractive index n_{eff} and acoustic phase velocity V_a, as follows:

$$\nu_B = \frac{2n_{\text{eff}} V_a}{\lambda} = \frac{2n_{\text{eff}}}{\lambda}\sqrt{\frac{E}{\rho}} \tag{6}$$

where E *is* the Young's modulus, and ρ is the equivalent density. It can obtained that $V_a \approx 3380$ m/s and $n_{\text{eff}} = 1.43$, numerically. Because the effective acoustic phase velocity of the first peak

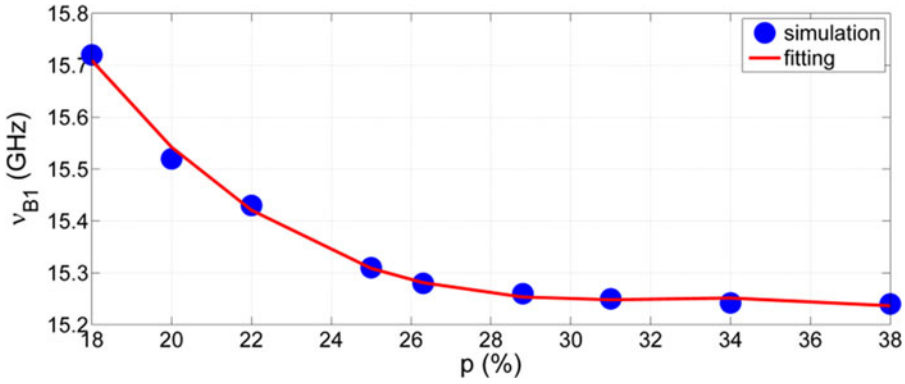

Fig. 5. Relationship between the Brillouin frequency shift of the first peak ν_{B1} and the air-fill fraction p at a certain launch position.

corresponding to the fundamental surface acoustic mode is lower than the one of the higher-order mode, ν_{Ba1} and ν_{Bb1} are smaller than ν_{Ba2} and ν_{Bb2}. The difference between Fig. 4(a) and (b) spectrums are due to the difference of equivalent air-fill fractions at the two launch positions in DOF: $p_a = 28.8\%$, and $p_b = 26.3\%$. In the cases of different local air-fill fractions, the equivalent density, acoustic phase velocity, and the effective refractive index may be different, then, due to (6), the BFS are different. When air-fill fraction increases, the effective velocity V_a decreases and thus the BFSs are downwards. Furthermore, the relationship between BFS of the first peak and air-fill fraction are shown in Fig. 5. In the case of an increasing air-fill fraction, the BFS ν_{B1} is reduced. This conclusion is also supported by the results of reported in [12].

4. Longitudinal Structural Fluctuations Evaluating

The BFS is sensitive to the air-fill fraction p. Then, the longitudinal uniformity along DOF can be monitored by a surface-BS based BOTDA. This proposed surface-BS based BOTDA is similar to current conventional BS based BOTDA, except that the BFS for surface-BS is smaller, due to the smaller acoustic phase velocity of SAW (~3380 m/s) than that of bulk acoustic wave (~5960 m/s [11]). The spatial resolution of surface-BS based BOTDA is also determined by the pulse duration. However, the SAWs are inherently sensitive to sub-wavelength surface defects or features [12], [13], therefore, the surface-BS is highly sensitive to the fiber air-hole micro-structures, compared with the traditional BOTDA technique, the surface-BS based BOTDA is more effective for evaluation longitudinal structural fluctuation of micro-structured optical fibers.

ν_{B1} and p versus distance along DOF at a certain launch position are shown in Fig. 6, with a spatial resolution of 1 m. There can be a higher spatial resolution in the practical applications, adapted to the longitudinal uniformity of DOF. In order to optimize the evaluating, the average sensitivity of ν_{B1} to p is defined as:

$$S_{\text{ave}} = \Delta\nu_{B1}/\Delta p \tag{7}$$

where $\Delta\nu_{B1}$ and Δp are the variation of ν_{B1} and p, respectively. For different launch positions, the average sensitivity S_{ave} may be different. The optimal S_{ave} can be obtained by demonstration the correlation between S_{ave} and p at different launch positions, as shown in Fig. 7. It is found that S_{ave} is reduced from 0.1 GHz/1% to 5×10^{-4} GHz/1%, when p is increased from 18% to 34%. It is suggested to choose a launch position with a smaller local air-fill fraction to obtain the higher average sensitivity of the BFS to the structural fluctuation. It is worth noting that we ignore the influences of the temperature and strain on BFS because of the short monitoring duration. What is more, due to the longitudinal non-uniformity, the surface-BS spectrum will be broadened. However, the broadening is accumulated by the non-uniformity at different longitudinal positions, randomly, therefore, it is hard to calculate this broadened linewidth precisely, in the numerically simulation. It

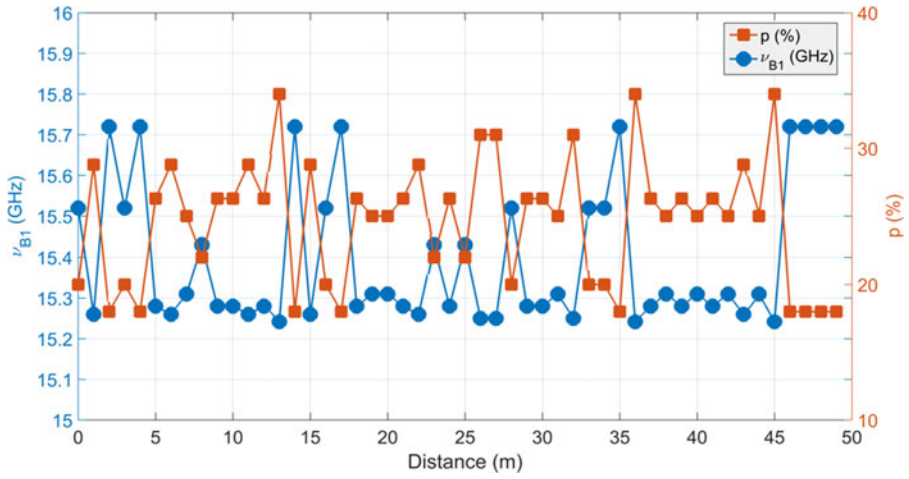

Fig. 6. Brillouin frequency shift of the first peak ν_{B1} and the air-fill fraction p versus distance along DOF at a certain launch position, with a spatial resolution of 1 m.

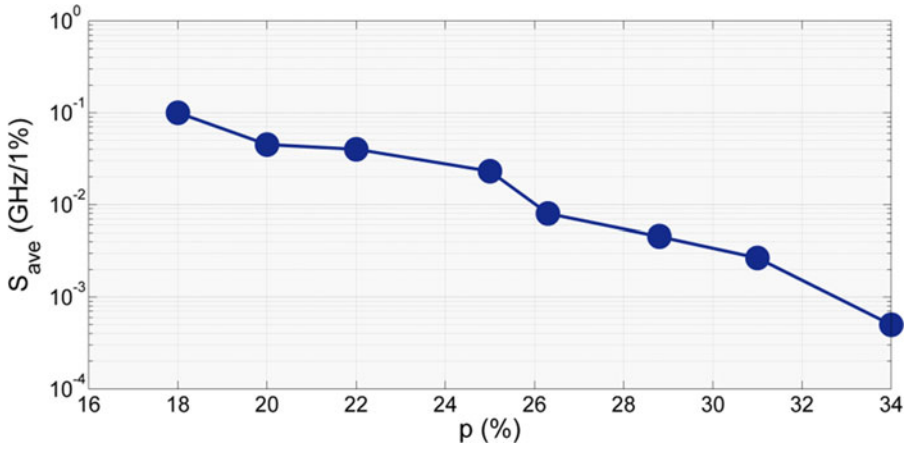

Fig. 7. The correlations between the average sensitivity S_{ave} and the local air-fill fraction p.

is suggested that, compared with the BFS, this linewidth broadening is not an effective function for longitudinal structural fluctuation evaluation, and in our simulation it is ignored.

5. Conclusion

The silica glass-air DOF is a novel optical fiber with random air-holes in the silica rod. A novel guide mechanism, i.e., TAL in DOF is numerically simulated and confirmed by FD-BPM. Then, the surface-BS characteristic in DOF is investigated by the equation of elasto-dynamics with electrostriction. It is found that there are two main peaks in the surface-BS spectrum and the BFS is sensitive to the air-fill fraction of DOF. Therefore, measurement of BFS by BOTDA can be considered as a potential solution of longitudinal structural fluctuations evaluating of DOF. The higher average sensitivity of BFS to the air-fill fraction can be obtained by employing the launch position with less air-fill fraction in practical application. This work extends both the concepts of DOF and TAL. Some experimental research including the fabrication of our simulated silica glass-air DOF, further confirmation of the surface-BS characteristics of DOF, update of the numerical model, and the optimization of longitudinal structural fluctuations evaluating, will be the subject of a future work.

Acknowledgments

The authors are grateful for Dr. Q. Liu for the help of the numerical simulation and helpful discussions.

References

[1] D. S. Wiersma, "Disordered photonics," *Nature Photon.*, vol. 7, no. 3, pp. 188–196, 2013.
[2] T. Schwartz, G. Bartal, S. Fishman, and M. Segev, "Transport and Anderson localization in disordered two-dimensional photonic lattices," *Nature*, vol. 446, no. 7131, pp. 52–55, 2007.
[3] L. Levi, Y. Krivolapov, S. Fishman, and M. Segev, "Hyper-transport of light and stochastic acceleration by evolving disorder," *Nature Phys.*, vol. 8, no. 12, pp. 912–917, 2012.
[4] S. Karbasi, C. R. Mirr, P. G. Yarandi, R. J. Frazier, K. W. Koch, and A. Mafi, "Observation of transverse Anderson localization in an optical fiber," *Opt. Lett.*, vol. 37, no. 12, pp. 2304–2306, 2012.
[5] S. Karbasi, C. R. Mirr, R. J. Frazier, P. G. Yarandi, K. W. Koch, and A. Mafi, "Detailed investigation of the impact of the fiber design parameters on the transverse Anderson localization of light in disordered optical fibers," *Opt. Exp.*, vol. 20, no. 17, pp. 18692–18706, 2012.
[6] S. Karbasi, T. Hawkins, J. Ballato, K. W. Koch, and A. Mafi, "Transverse Anderson localization in a disordered glass optical fiber," *Opt. Mater. Exp.*, vol. 2, no. 11, pp. 1496–1503, 2012.
[7] M. Chen and M. J. Li, "Observing transverse Anderson localization in random air line based fiber," *Proc. SPIE*, vol. 8994, 2014, Art. no. 89941S.
[8] S. Karbasi, K. W. Koch, and A. Mafi, "Multiple-beam propagation in an Anderson localized optical fiber," *Opt. Exp.*, vol. 21, no. 1, pp. 305–313, 2013.
[9] A. Mafi, S. Karbasi, W. K. Koch, T. Hawkins, and J. Ballato, "Transverse Anderson localization in disordered glass optical fibers: A review," *Materials*, vol. 7, no. 8, pp. 5520–5527, 2014.
[10] A. Mafi, "Transverse Anderson localization of light: A tutorial," *Adv. Opt. Photon.*, vol. 7, no. 3, pp. 459–515, 2015.
[11] B. Stiller *et al.*, "Photonic crystal fiber mapping using Brillouin echoes distributed sensing," *Opt. Exp.*, vol. 18, no. 19, pp. 20136–20142, 2010.
[12] J. C. Tchahame, J.-C. Beugnot, K. P. Huy, V. Laude, A. Kudlinski, and T. Sylvestre, "Surface Brillouin scattering in photonic crystal fibers," *Opt. Lett.*, vol. 41, no. 14, pp. 3269–3272, 2016.
[13] J.-C. Beugnot, S. Lebrun, G. Pauliat, H. Maillotte, V. Laude, and T. Sylvestre, "Brillouin light scattering from surface acoustic waves in a subwavelength-diameter optical fibre," *Nature Commun.*, vol. 5, 2014, Art. no. 5242.
[14] O. Florez *et al.*, "Brillouin scattering self-cancellation," *Nature Commun.*, vol. 7, 2016, Art. no. 11759.
[15] P. Zhang, J. Zhang, P. Yang, S. Dai, X. Wang, and W. Zhang, "Fabrication of chalcogenide glass photonic crystal fibers with mechanical drilling," *Opt. Fiber Technol.*, vol. 26, Part B, pp. 176–179, 2015.
[16] P. Falkenstein, C. D. Merritt, and B. L. Justus, "Fused preforms for the fabrication of photonic crystal fibers," *Opt. Lett.*, vol. 29, no. 16, pp. 1858–1860, 2004.
[17] Z. Guiyao, H. Zhiyun, L. Shuguang, and H. Lantian, "Fabrication of glass photonic crystal fibers with a die-cast process," *Appl. Opt.*, vol. 45, no. 18, pp. 4433–4436, 2006.
[18] K. Cook *et al.*, "Air-structured optical fiber drawn from a 3D-printed preform," *Opt. Lett.*, vol. 40, no. 17, pp. 3966–3969, 2015.
[19] W. P. Huang and C. L. Xu, "Simulation of three-dimensional optical waveguides by a full-vector beam propagation method," *IEEE J. Quantum Elect.*, vol. 29, no. 10, pp. 2639–2649, Oct. 1993.
[20] J. C. Butcher, *Numerical Methods for Ordinary Differential Equations*, 2nd ed. Hoboken, NJ, USA: Wiley, 2008.
[21] H. De Raedt, A. Lagendijk, and P. de Vries, "Transverse localization of light," *Phys. Rev. Lett.*, vol. 62, no. 1, pp. 47–50, 1989.
[22] G. R. Hadley, "Transparent boundary condition for the beam propagation method," *IEEE J. Quantum Elect.*, vol. 28, no. 1, pp. 363–370, Jan. 1992.